

**Solution-processed, vertically stacked hetero-structured diodes based on
liquid-exfoliated WS₂ nanosheets: From electrode- to bulk-limited behavior**

Shixin Liu, Er-Xiong Ding, Adam G. Kelly, Luke Doolan, Cian Gabbett, Harneet
Kaur, Jose Munuera, Tian Carey, James Garcia, Jonathan N. Coleman*

*School of Physics, CRANN & AMBER Research Centres, Trinity College Dublin,
Dublin 2, Ireland*

*colemaj@tcd.ie (Jonathan N. Coleman); Tel: +353 (0) 1 8963859.

Supplementary materials

- S1 Experimental details
- S2 AFM characterization
- S3 Optical characterization of materials
- S4 Optical characterization of sprayed WS₂ film
- S5 Cross-sectional SEM images and porosity estimation
- S6 Electrode resistance calculation and subtraction
- S7 Comparison of devices with and without AgNWs
- S8 Photograph of an ITO/WS₂/ITO lateral device
- S9 J - V curves of Ohmic devices with various WS₂ film thickness
- S10 J/E - E curves of ITO/WS₂/I-SWNTs/AgNWs devices
- S11 Original J - V curves of ITO/WS₂/S-SWNTs devices
- S12 Corrected J - V curves of ITO/WS₂/S-SWNTs devices
- S13 Rectification ratio
- S14 Conduction mechanism and fittings of ITO/WS₂/S-SWNTs devices
- S15 The extracted saturation current density J_s from fitting
- S16 On the hysteresis of Schottky devices
- S17 WS₂ film roughness measured by profilometry
- S18 Transition film thickness from electrode-limited to bulk-limited behaviors

S1 Experimental details

Material preparation

WS₂ dispersion was prepared by probe sonicating the powder (Alfa Aesar, 99.9%) in IPA (HPLC grade). The powder was mixed with IPA with a concentration of 30 mg/mL in a metal beaker and being sonicated by a replaceable head tip for 1 h at 40% amplitude with a pulse of 6 s on and 2 s off. The dispersion was centrifuged at 2 krpm for 1 h and the supernatant was discarded. The sediment was re-dispersed with IPA and being sonicated for 8 h at 40% amplitude with a pulse of 6 s on and 2 s off. The metal beaker was kept in water bath cooling during sonication. The size-selection of nanosheets was done by liquid cascade centrifugation method. First, the dispersion was subjected to 2 krpm centrifugation for 2 h and the supernatant was collected. Then, the supernatant was further centrifuged at 6 krpm for 2 h and the sediment after centrifugation was collected and re-dispersed with IPA as the WS₂ ink for further characterizations and device fabrication.

SWNTs aqueous dispersion was prepared by sonicating P3-SWNTs (Carbon Solution) in an aqueous surfactant solution. 20 mg SWNTs powder was dispersed in 40 mL deionized water containing 200 mg sodium dodecyl benzene sulfonate (SDBS, Sigma-Aldrich, technical grade). The dispersion was sonicated by a tapered tip for 0.5 h at 30% amplitude with a pulse of 3 s on and 3 s off. The dispersion was then centrifuged for 2 h at 6 krpm. The supernatant was collected for device fabrication.

SWNTs IPA dispersion was obtained by probe-sonicating 2 mg P3-SWNTs powder in 40 mL IPA for 4 h at 30% amplitude with a pulse of 3 s on and 3 s off. The final dispersion was used without centrifugation.

AgNWs IPA dispersion (Sigma-Aldrich, 5 mg/mL in IPA, diameter 40 nm and length 35 μ m) was diluted in IPA with a concentration of about 0.5 mg/mL.

Device fabrication

Indium tin oxide (ITO) coated glass substrate (Ossila, 20 Ω sq⁻¹) was used as bottom

electrode. To pattern it, Kapton tape was used to cover the ITO surface and the substrate was immersed in diluted hydrochloride acid (Sigma-Aldrich, ACS reagent, 37%) aqueous solution at 80 °C for 5 min. The etched ITO glasses were cleaned with Hellmanex aqueous solution, water, and IPA sequentially in sonic bath for 10 min each. The substrates were blow dried by a stream of nitrogen gas. The glass substrates were cleaned in the same way.

A Harder and Steenbeck Infinity airbrush was attached to a Janome JR2300N mobile gantry to spray the dispersion over a programmed area at a line speed of 5 mm/s. The spraying process was done in ambient conditions. The dispersion (except AgNWs) was sonicated in sonic bath for 10-20 min before spraying. The AgNW dispersion was briefly sonicated and shaken before spraying. The WS₂ film was obtained by spraying ~1 mg/mL WS₂ dispersion on solvent-cleaned ITO at 100 °C with a spray rate of ~0.5 mL/min. The films were annealed at 200 °C in glovebox ([O₂]/[H₂O] < 0.8 ppm) for 30 min and were allowed to cool down naturally before depositing top electrodes. A laser-cut aluminum shadow mask was used to deposit top electrode. It was placed on the substrate and its position was fixed by attaching Kapton tape around the mask onto the substrate. The hotplate was set to 150 °C for SWNTs and AgNWs IPA dispersion and 250 °C for SWNTs aqueous dispersion. Due to the effective cooling of the nitrogen gas flow, the temperature of substrates on the hotplate during spraying never exceeds 100 °C measured with a thermocouple. 2 mL 0.05 mg/mL SWNTs IPA dispersion was sprayed at a rate of ~0.1 mL/min, while 0.5 mL 0.5 mg/mL aqueous dispersion was sprayed at a rate of ~0.015 mL/min. The final devices were annealed at 80 °C for 30 min in glovebox and left overnight to remove residual solvents and stabilize the performance. Devices with AgNWs were further annealed at 120 °C for 15 min to fuse the junctions. No additional surface treatment was conducted except annealing. The device area was defined as the overlapping region between ITO, WS₂, and top electrodes, which is about 2-4 mm².

Characterizations

UV-Vis-NIR spectroscopy: The UV-Vis-NIR extinction spectra of WS₂ and SWNTs dispersions were collected with Cary 1050 with a 10 mm optical length cuvette. An integration sphere was utilized during the collection of the absorption spectra. The collected extinction and absorption spectra of WS₂ and SWNTs were subtracted by their corresponding solvent spectra.

Raman spectroscopy: The Raman spectra were acquired using the Renishaw inVia Raman microscope. A laser with a wavelength of 532 nm (laser power approximately 1.5 mW) was used to excite the sample using a 100X objective. A grating of 1800 grooves/mm is used to disperse the signal onto the detector. The sample for the Raman spectroscopy were prepared by drop-casting the dispersion on pre-heated silicon wafers coated with 300 nm of silicon dioxide.

AFM: AFM was performed using a Bruker Multimode 8 microscope to determine the dimensions of WS₂ flakes and SWNTs. Materials after dilution and bath-sonication were drop-cast onto Si/SiO₂ and annealed to remove residual solvent. The samples were scanned using OLTESPA R3 cantilevers in ScanAsyst mode. We use Gwyddion software to process our data. We plane level the scans and align the rows using the median of differences to remove AFM artefacts such as scanner bow and tilt. Finally, we extract a height and length profile across 50 I-SWNT and S-SWNT to determine L_{NT} and D_{NT}. The length and thickness of WS₂ were extracted with more than 100 nanosheets.

TEM: For TEM imaging, a JEOL 2100 microscope operated at an accelerating voltage of 200 kV was used. The grids were prepared by drop-casting 10 ul of dispersion (approx. concentration 0.2 mg/ml) on Holey carbon grids (400 mesh). The grids were dried in a vacuum oven at 70 °C overnight prior to the TEM observation.

SEM: The SEM images were collected by a Zeiss Ultra Plus at accelerating voltages of 2 kV.

FIB-SEM: The cross-sectional images of devices were obtained by a Zeiss Auriga dual-beam FIB-SEM microscope. The accelerating voltage was 30 kV.

Electrical measurement: The I - V characteristics were collected in ambient environment under dark conditions by using the Suss probe station connected with Keithley 2612A from -3 to 3 V (the first sweep) and from 3 to -3 V (the second sweep). There was no pause between these two sweeps.

Scanner: The sprayed WS₂ film on glass was optically scanned by an Epson Perfection V700 photo flatbed scanner. The spatial resolution is 6400 dpi and spectral resolution is 48 bit. The point resolution of the image is about 4 μm .

Profilometry: The thickness and average roughness of films were measured by a Bruker Dektak profilometer. The line profile was taken with 2000 μm length and a resolution of ~ 100 nm/sample. More than 4 profiles were taking for each sample and the obtained thickness and roughness were further averaged to find their mean values.

S2 AFM characterization

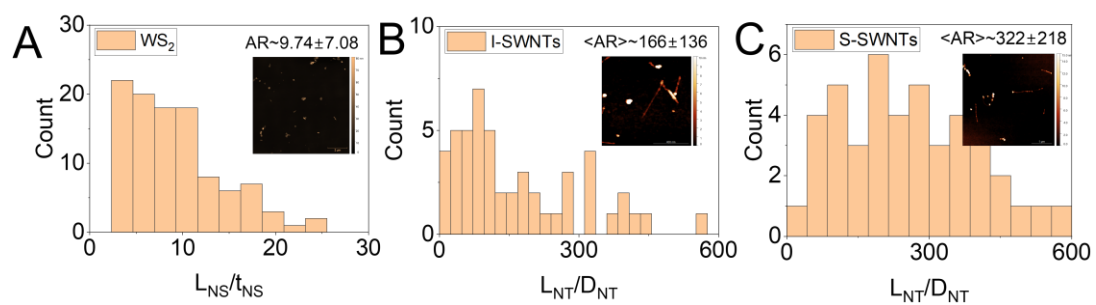


Fig. S1 (A-C) The histogram plots of aspect ratio of nanosheets and nanotubes. AFM images of WS_2 , I-SWNTs and S-SWNTs are shown in the corresponding insets, respectively.

S3 Optical characterization of materials

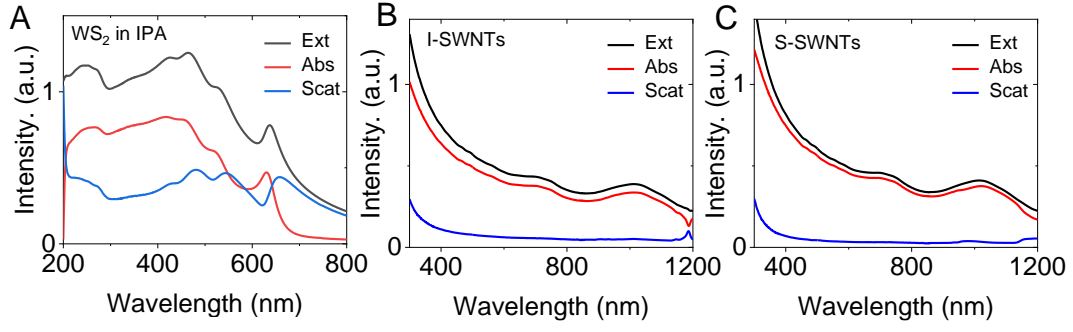


Fig.S2 UV-Vis-NIR spectra of WS₂ in IPA (A), I-SWNTs (B), and S-SWNTs (C) dispersions.

Once the extinction spectrum of WS₂ is obtained, the number of layers $\langle N_{NS} \rangle$ and the length of the nanosheet $\langle L_{NS} \rangle$ can be estimated by the following equations¹. $\langle N_{NS} \rangle$ be obtained by equation (1).

$$\langle N_{NS} \rangle = 6.35 \times 10^{-32} e^{\lambda_A / 8.51} \quad (1)$$

where λ_A is the wavelength of A-exciton extinction peak. Further, $\langle L_{NS} \rangle$ can also be obtained by equation (2) using extinction peak intensities at 235 nm and 290 nm as below.

$$\langle L_{NS} \rangle = \frac{2.3 - Ext_{235} / Ext_{290}}{0.02 Ext_{235} / Ext_{290} - 0.0185} \quad (2)$$

where Ext_{235} and Ext_{290} correspond to the extinction intensity at 235 nm and 290 nm, respectively. Although the equation is more accurate for WS₂ prepared in sodium cholate/H₂O solution, the obtained $\langle N_{NS} \rangle$ and $\langle L_{NS} \rangle$ are close to the values found from AFM.

S4 Optical characterization of sprayed WS₂ film

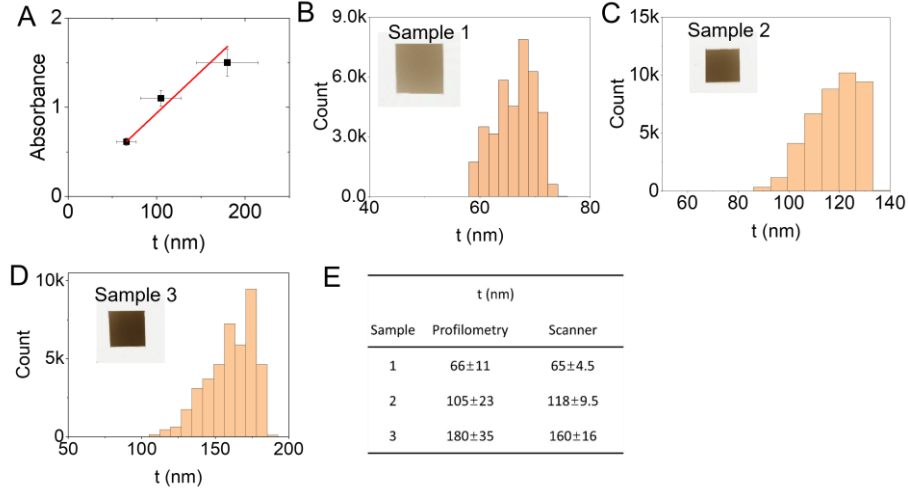


Fig. S3 (A) The mean absorbance extracted from the scanned images against film thickness measured by profilometry. (B-D) The histogram plot of thickness and scanned images in insets extracted from Image J for sprayed WS₂ film on a glass slide, (E) Comparison of film thickness obtained by profilometry and optical scanner.

The sprayed WS₂ film was optically scanned. The obtained image was uploaded into Image J and split into 3 channels: red, green, and blue. The blue image was kept and used further as it allows minimum interference fringes with glass. The image was then opened by Origin and converted into data matrix. There were ~2000 columns of data obtained after conversion and we picked 20 columns for every 100 columns. These columns were combined into one column. These optical signal values were converted into transmittance using the following equation (3):

$$T = -0.01622 + (4.2922 \times 10^{-6} S) + (1.6598 \times 10^{-10} S^2) \quad (3)$$

where S is the optical signal and T is the transmittance. The transmittance of glass substrate was obtained following the above step and the mean transmittance of the glass substrate T_{glass} is obtained to be 88.91%. The transmittance of WS₂ film T_{WS_2} is obtained by $T_{WS_2+glass} / T_{glass}$. The absorbance A can be obtained by using $A = -\lg T$.

The mean A for three films with different thicknesses t were obtained and plotted against t measured by profilometry in Fig. S3(A). As A should scale linearly with t , it allows us to find the following equation (4):

$$t = \frac{A}{9.34 \times 10^{-2}} \quad (4)$$

The absorbance for each sample was converted into t by using equation (4). The histogram plots of 3 samples are shown in Fig. S3B-D. The mean film thicknesses $\langle t \rangle$ determined by profilometry and optical scanner are shown in Fig. S3E. The thickness for each sample is close measured by these two methods.

For the thinnest sample, despite there is some variation in film thickness, the scanner does not detect any regions thinner than ~ 60 nm suggesting a low probability of large-sized pinholes.

S5 Cross-sectional SEM images and porosity estimation

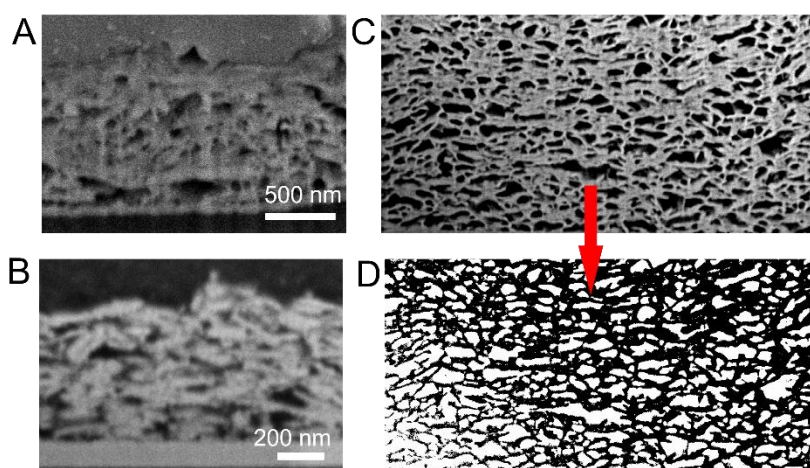


Fig.S4 Cross-sectional SEM image of ITO/WS₂/I-SWNTs/AgNWs (A) and ITO/WS₂/S-SWNTs (B). (C) Cross-sectional SEM image of WS₂ network and its binary image (D).

The cross-sectional SEM images of devices with thin WS₂ network are shown in Fig. S4 (A) and (B). The thicknesses of WS₂ are 700 and 580 nm, respectively in these two images. The measured WS₂ thicknesses by profilometer are 680 and 544 nm, which are close to these values.

The cross-sectional image of thick WS₂ network was imported into ImageJ. The brightness/contrast of the image was auto-adjusted and is shown in Fig. S4C. Then, the image was converted into binary image where white area represents pores and black area represents nanosheets. Using measure function, the percentage of white area was obtained to be 56%, which could be regarded as an estimation of porosity. Such porosity is close to the value of ~ 50% estimated by the film density method².

S6 Electrode resistance calculation and subtraction

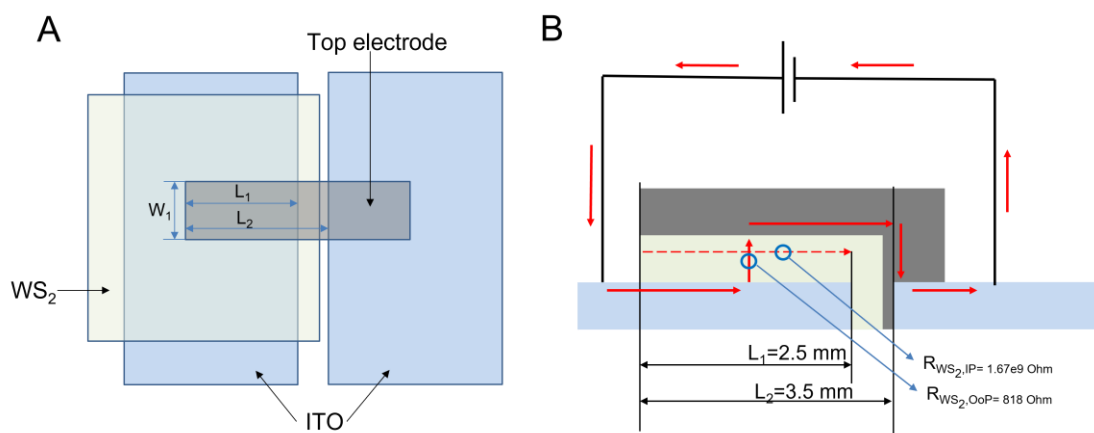


Fig. S5 An illustration of device dimensions, (A) top view and (C) cross-section view and the red arrows represent the current flow direction.

The electrode resistance will depend on its conductivity σ_e and dimensions (length, width, and thickness). First, σ_e was obtained by a two-probe measurement with identical electrode films sprayed on glass slides as on devices. Then, dimensions of these films such as length L , width W , and thickness t were measured. The σ_e can be obtained by $\sigma_e = L / (R_e W t)$ and are 1.8×10^3 S/m for 80 nm I-SWNTs, 6.8×10^3 S/m for 650 nm S-SWNTs, 4.8×10^5 S/m for 260 nm I-SWNTs/AgNWs and 4.8×10^5 S/m for 100 nm ITO (quoted value). We can find the first two electrodes are much less conductive than the latter two. It is important to find out how much influence of these electrodes' resistance can impose on the total device resistance R_{total} , which is given by $R_{total} = R_c + R_{WS_2} + R_e$, where R_c is the contact resistance, R_{WS_2} is the WS₂ resistance, and R_e is the electrode resistance. The device area A is defined as $A = L_1 W_1$.

Next, we find the actual electrode dimensions by comparing the OoP and IP resistance from WS₂ and finding the charge/current transporting route. A schematic demonstration of the top view of the device dimensions is shown in Fig. S5A as well as its cross-sectional schematic showing the current flow indicated by red arrows (Fig. S5B). Using the mean conductivity $\langle \sigma_{OoP} \rangle \sim 1.63 \times 10^{-4}$ S/m and $\langle \sigma_{IP} \rangle \sim 2 \times 10^{-3}$ S/m of WS₂ given in the manuscript, and device dimensions ($L_1 = 2.5$ mm and $W_1 = 1.5$ mm),

we can find the OoP and IP resistance ($R_{WS_2, OoP}$ and $R_{WS_2, IP}$) for WS_2 will be 818 Ohm and 1.67×10^9 Ohm, respectively, for a 500 nm thick WS_2 film. This large OoP and IP resistance difference indicates the charge will preferably flow from ITO along the OoP direction of WS_2 to the top SWNTs electrode and is not likely to flow horizontally along WS_2 layer. Then, the charge will flow laterally along the top electrode to the other ITO. The longest distance current can flow through the electrode is L_2 (all the way from the end) while the shortest distance is $L_2 - L_1$ (only from the nearest edge of the active area of the device). Assuming the OOP current through the WS_2 flows through the entire device area, then the average distance current flows through the top electrodes is $L_2 - L_1 / 2$. Using this value means we are assuming that the current flows vertically in a reasonably uniform manner throughout the area of the WS_2 film defined by the electrodes (we justify this assumption below).

Then we can estimate R_e using $R_e = \frac{L_2 - L_1 / 2}{\sigma_e W_1 t}$

Using the above conductivities for each type of electrodes and an electrode dimension $L_2 - L_1 / 2 = 2.25$ mm and $W_1 = 1.5$ mm, we can obtain R_e for I-SWNTs, S-SWNTs, I-SWNTs/AgNWs, and ITO electrodes can be calculated to be 1×10^4 , 340, 12.2, and 29.8 Ohm, respectively. Comparing with $R_{WS_2, OoP} \sim 818$ Ohm, one can easily see that I-SWNTs/AgNWs and ITO electrodes would impose a small influence on the resistance of the whole device and its influence could be ignored. However, R_e from I-SWNTs is much too large to be useable. In addition, R_e from S-SWNTs (340 Ohm), although smaller than R_{WS_2} at all WS_2 thickness (minimum value 818 Ohm) cannot be ignored if we want to obtain accurate results. Although R_e could always be reduced by increasing electrode thickness, we deliberately avoided to spray much solvent on top of nanosheet network in case the network may be damaged by the compressed nitrogen flow or the re-dispersing problem in case the solvent dried slowly.

Because of the discussion above, we did not use I-SWNTs as electrodes, instead using

I-SWNTs/AgNWs (assuming R_e for I-SWNTs/AgNWs based devices could be neglected). In the case of S-SWNTs based devices, we find R_e for S-SWNTs using the equation above and then subtracted this from the total device resistance to find the correct WS₂ resistance.

Justification of the assumption that the current flows vertically throughout the area of the WS₂ film in a reasonably uniform manner

In our systems, especially the devices with I-SWNTs top electrodes, the top electrode resistance is relatively high compared to an evaporated/sputtered metal electrode. Then there is a concern that the current density through the WS₂ might be larger on the side where the top electrode first meets the WS₂, with the vertical current density falling off further into the film. Such a spatial variation in vertical current density would be driven by the predilection of the current to take the path of least resistance. this scenario is illustrated in Fig. S6A. If the current density were to decay rapidly with distance into the film (from right to left) then the majority of current flow would be on the extreme right-hand side of the WS₂ film. In that case it would be inappropriate to use the area of electrode overlap as the active area of the WS₂. Alternatively, if the current density were to decay very slowly with distance into the film, one could approximate the current flow as uniform throughout the active area of the WS₂. Although such behavior could be analyzed using a transmission line model, we take a simpler approach to demonstrate that transmission line analysis is not necessary.

To do this, we model a simplified scenario of current flow we divide the active area of WS₂ into two regions, one on the right where there is a uniform current flow, and one on the left where no current flows. We labeled the depth of the region where current flows as a λ as shown in Fig. S6B. For example, if the current density decayed exponentially with distance into the film, then λ would be equivalent to the decay length.

Under these circumstances the resistance of the system is there's some of the horizontal resistance associated with top electrode and vertical resistance associated with the region through which current flows (neglecting the very low resistance associated with the bottom electrode). This means:

$$R_{total} = R_{WS_2} + R_e \quad (5)$$

$$R_{total} = \frac{t_d}{\sigma_{OoP,WS_2} W_1 a} + \frac{L_2 - L_1 + a / 2}{\sigma_e W_1 t} \quad (6)$$

This equation shows that increasing a (so the current occupies more of the active area) increases the resistance associated with the current flowing through the top electrode. Decreasing a increases the resistance associated with the current flowing through the WS_2 .

We propose that the extent of the active WS_2 area through which current flows, represented by the parameter a , can be found by minimizing R_{total} , ie when $dR_{total} / da = 0$.

Differentiating yields

$$\frac{dR_{total}}{da} = -\frac{t_d}{\sigma_{OoP,WS_2} W_1 a^2} + \frac{1}{2\sigma_e W_1 t} \quad (7)$$

When this derivative is zero defines the value of a consistent with the minimal resistance, a_{min} :

$$a_{min} = \sqrt{\frac{2\sigma_e t t_d}{\sigma_{OoP,WS_2}}} \quad (8)$$

Taking $\sigma_{OoP,WS_2} = 1.8 \times 10^{-4}$ S/m and the electrode conductivities and conductivities given above allows us to calculate a_{min} versus $t_d = 500$ nm for the two top electrode

types used. These graphs are plotted in Fig. S6C. In all cases, we find that a_{min} is larger than the length of the active device area, L_1 (2.5 mm). This means that the resistance is minimized by the current flowing through the entire active area of the device. This justifies our initial assumption.

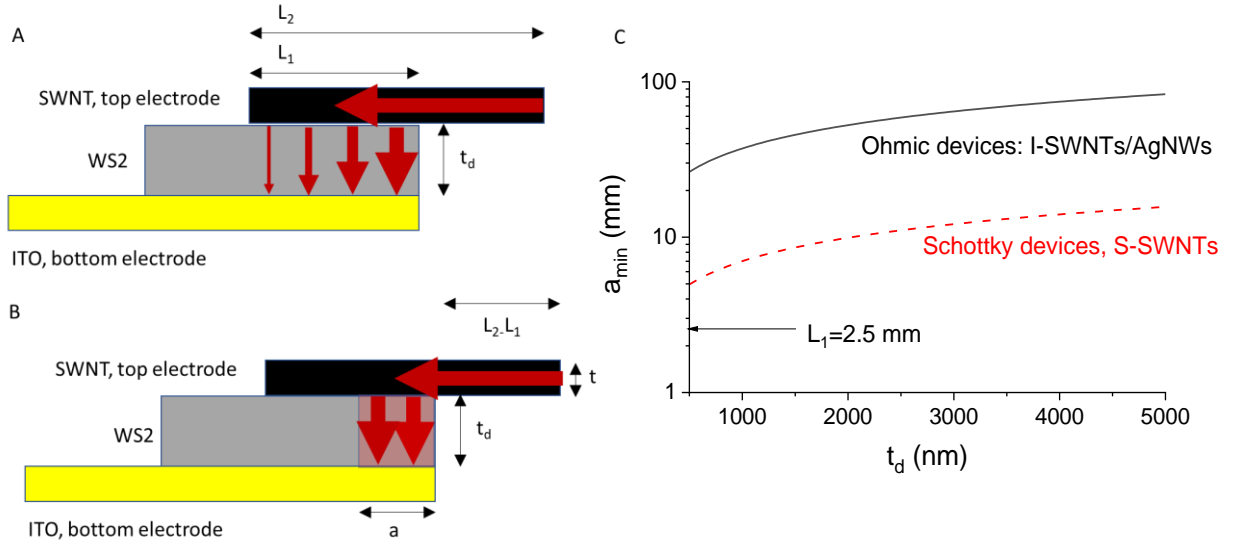


Fig. S6: (A,B) schematics showing current density decaying across the device (A) and a simplified approximation showing constant current flowing through a localized region of the device of depth a . C) Calculated values of a which minimize the device resistance as a function of WS_2 thickness.

S7 Comparison of devices with and without AgNWs

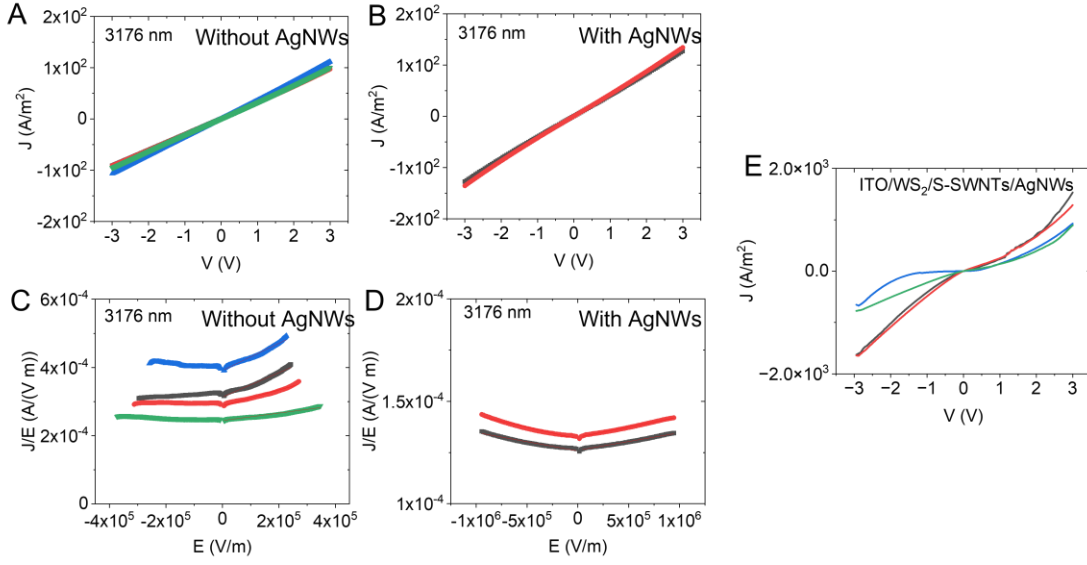


Fig. S7 J - V curves of ITO/3176 nm WS_2 /I-SWNTs (A) and ITO/3176 nm WS_2 /I-SWNTs/AgNWs (B), and their corresponding J/E - E curves for parameter extractions (C and D), respectively. (E) J - V curves of ITO/ WS_2 /S-SWNTs/AgNWs.

One example is shown with an Ohmic device with and without AgNWs on top. Fig. S7A-B show J - V curves of ITO/3176 nm WS_2 /I-SWNTs device to demonstrate the case without and with AgNWs and their corresponding J/E - E curves (Fig.S7 C-D). J - V curves remain symmetrical in absence of AgNWs. J with AgNWs tends to be higher, which proves that the voltage drop on electrode V_e can have an influence on J - V curves. The voltage drop on WS_2 can be obtained by $V_{WS_2} = V_{device} - V_e = V_{device} - R_e I$. The electric field E for WS_2 can be estimated by dividing V_{WS_2} to its t . The J/E - E curves without AgNWs were obtained by subtracting V_e first. It is found that the curve was not symmetrical probably due to current loss along with the top electrode. The σ_{OoP} and μ_{OoP} of WS_2 determined from these curves on the right side in Fig. S7C are 3.09×10^{-4} S/m and 1.37×10^{-1} $cm^2/(Vs)$, respectively. However, once we spray AgNWs on top to increase electrodes' conductivity, J/E - E curves remain symmetrical as expected and the extracted σ_{OoP} and μ_{OoP} are 1.29×10^{-4} S/m and 4.8×10^{-3} $cm^2/(Vs)$, respectively. The conductivity from these two methods is comparable but mobility shows a relatively larger difference. The result shows that the first method could result in a large difference for mobility while using

I-SWNTs/AgNWs double layered electrode could enable us to obtain consistent result with various thicknesses (Fig.3F and G in the main text).

Fig. S7E is J - V curves for ITO/WS₂/S-SWNTs/AgNWs. No rectifying behaviors were observed, and the curves are roughly symmetric. These behaviors will very likely happen due to the top electrode fabrication method. During spraying the top electrode, the ink droplets will be carried by the nitrogen gas flow. As there is space between the shadow mask and WS₂ film, ink flow will go underneath the mask and spread on WS₂ network. Thus, this results in an undesired contact between AgNWs and WS₂ at the edge of the electrode. To say it clearly, WS₂/S-SWNTs and WS₂/AgNWs interfaces exist at the same time for such devices. As AgNWs could make Ohmic contact with WS₂ and S-SWNTs would make Schottky contact with WS₂, the device will behave like neither Ohmic nor Schottky, which is exactly what observe in the below figure. However, this problem can be solved in the future by using other printing method with better resolution control on the printing features.

S8 Photograph of an ITO/WS₂/ITO lateral device

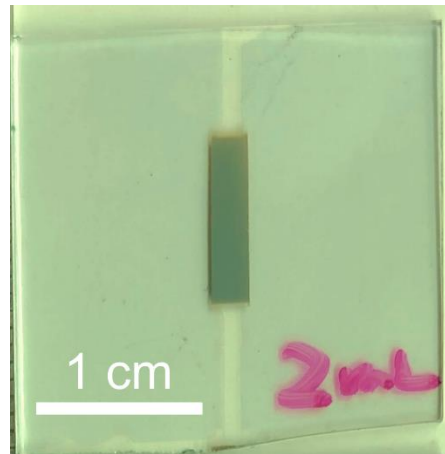


Fig. S8 Photograph of a lateral ITO/WS₂/ITO device.

S9 J - V curves of Ohmic devices with various WS_2 film thickness

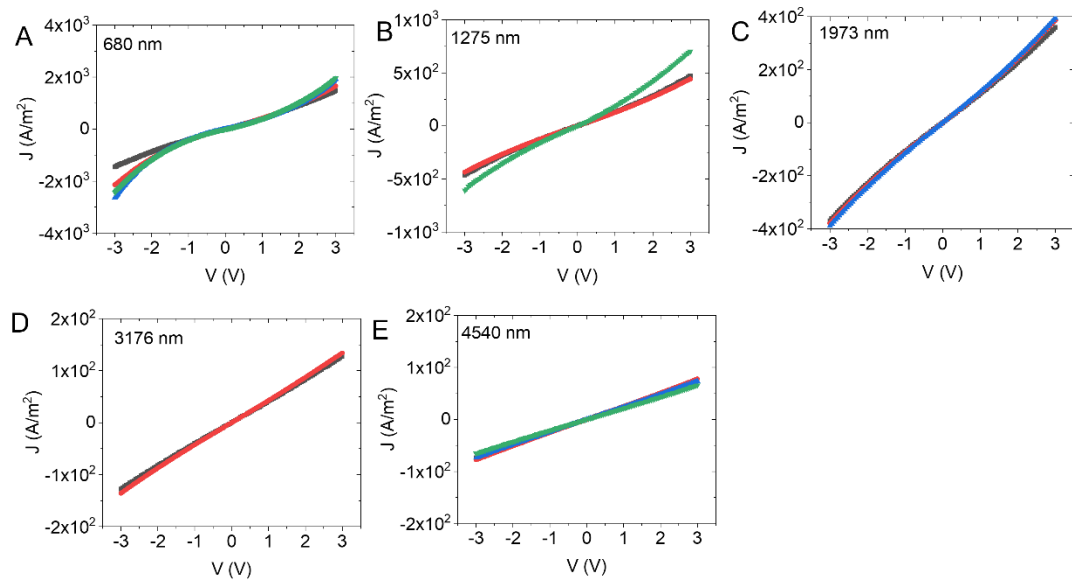


Fig. S9 J - V curves of ITO/ WS_2 /I-SWNTs/AgNWs with various WS_2 film thicknesses. The film thickness is indicated in each figure.

S10 $J/E - E$ curves of ITO/WS₂/I-SWNTs/AgNWs devices

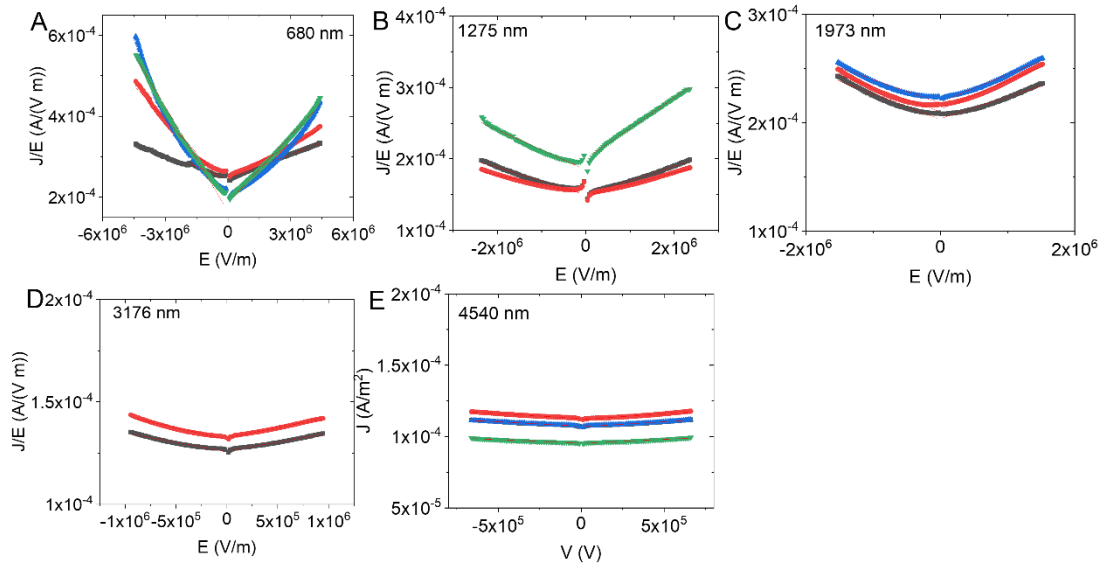


Fig. S10 $J/E - E$ curves of ITO/WS₂/I-SWNTs/AgNWs with various WS₂ film thicknesses. The film thickness is indicated in each figure.

S11 Original J - V curves of ITO/WS₂/S-SWNTs devices

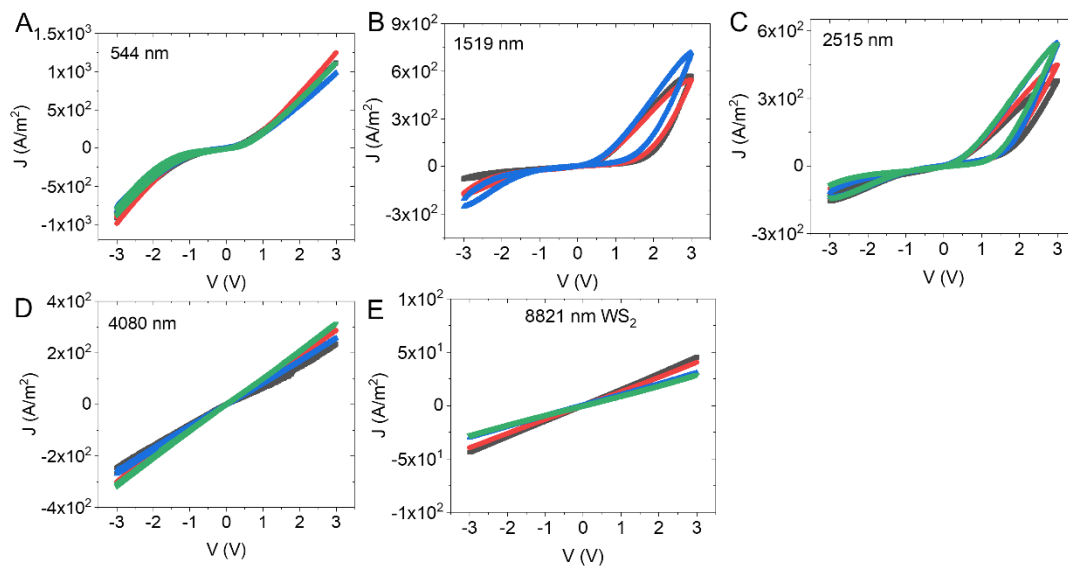


Fig. S11 Original J - V curves of ITO/WS₂/S-SWNTs with various WS₂ film thicknesses. The film thickness is indicated in each figure.

S12 Corrected J - V curves of ITO/WS₂/S-SWNTs devices

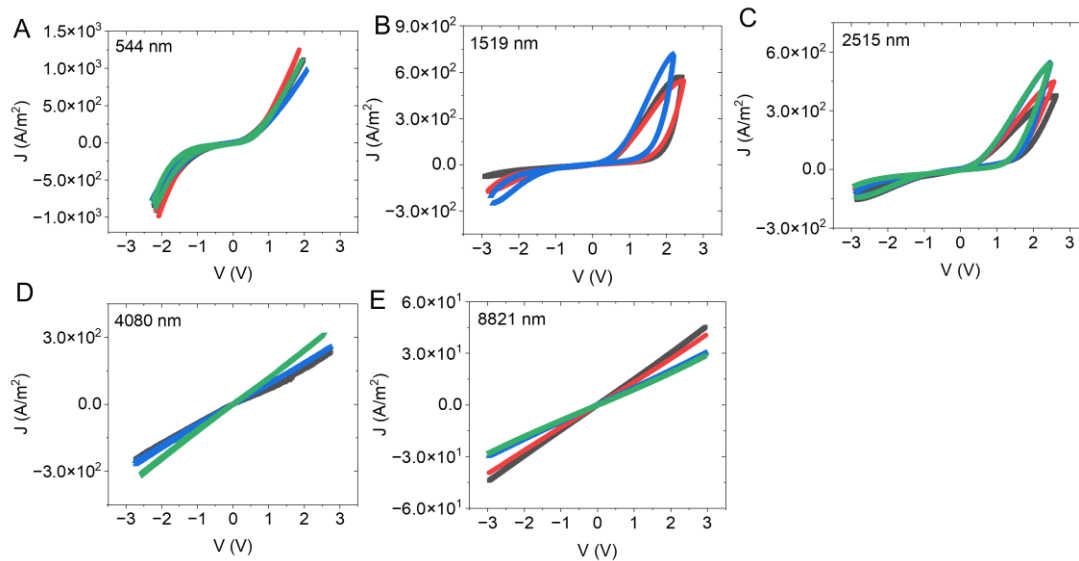


Fig. S12 J - V curves of ITO/WS₂/S-SWNTs with various WS₂ film thicknesses after subtracting the voltage drop due to electrode resistance. The film thickness is indicated in each figure.

S13 Rectification ratio

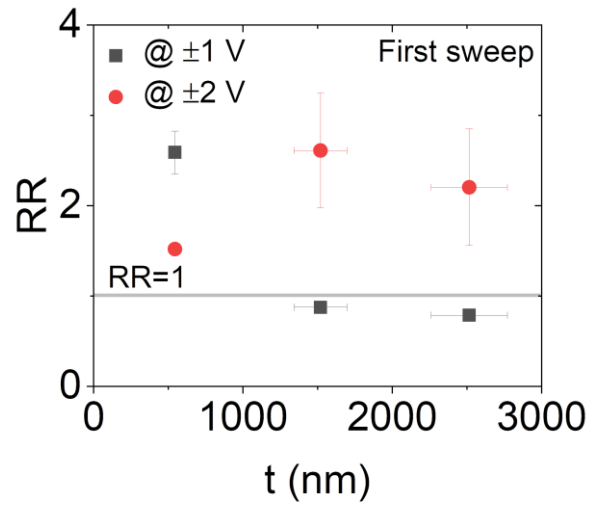


Fig. S13 Rectification ratio at ± 1 and ± 2 V for the first sweep

The rectification ratio for the first sweep is shown in Fig. S12. at ± 1 V, the thinnest device has a RR of ~ 2.5 , while 1.5 and 2.5 μm WS_2 thick devices have RR of ~ 1 . At ± 2 V, RR increases and approaches 3 for the latter two devices. Such behavior comes from the hysteresis of the device and results in a higher turn on voltage for the first sweep. Thus, we could barely observe rectification at lower biases.

S14 Conduction mechanism and fittings of ITO/WS₂/S-SWNTs devices

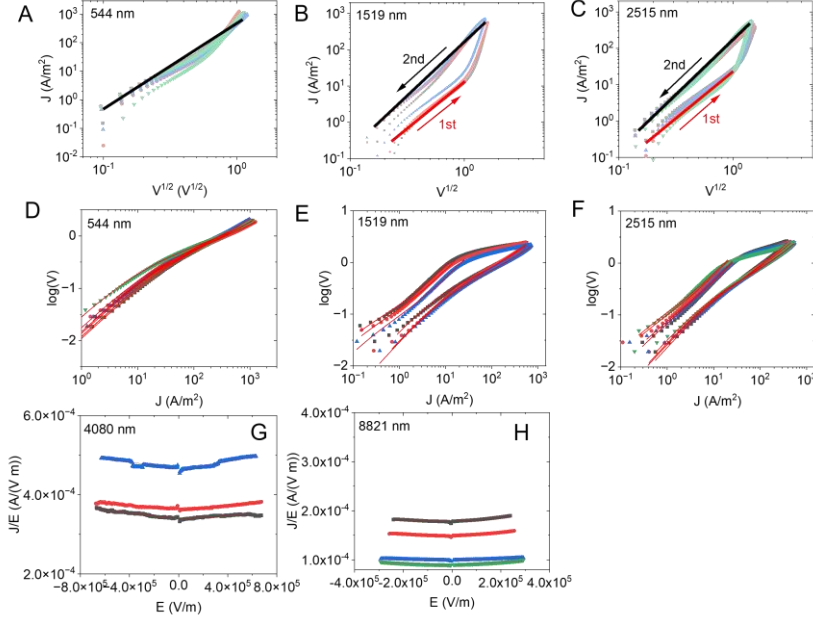


Fig. S14 $J-V^{0.5}$ curves (A-C), $\log(V)-J$ curves (D-F) and $J/E-E$ curves (G and H) of ITO/WS₂/S-SWNTs devices with various WS₂ film thicknesses. The film thickness is indicated in each figure

For devices exhibiting rectifying behaviors, we observed obvious hysteresis especially for ~ 1.5 and ~ 2.5 μm thick WS₂ ones. The conduction mechanism was firstly investigated. As shown in Fig. S14 A-C, a linear dependence of $J-V^{0.5}$ would indicate if the device were dominated by the thermionic emission (TE)³. We can find this linear dependence from roughly 0 to 1 V for the 1st sweep and from 0 V to the maximum bias V_{max} for the 2nd sweep. The curve for the 1st sweep from 1 V to V_{max} is obviously deviated from TE conduction. Thus, we used equation (7) which is given in the main text to fit the Schottky curves. The fitting was conducted above thermal voltage $3kT/q=25$ mV in all cases. As the hysteresis for the 544 nm thick WS₂ device was weak and almost entirely followed TE at ~ 25 mV- V_{max} , its $J-V$ curves were fitted to the entire range. For the ~ 1.5 and ~ 2.5 μm thick devices, their curves were fitted from ~ 25 mV to 1 V for the 1st sweep and were fitted from ~ 25 mV to V_{max} for the 2nd sweep. The fittings can be successfully done and are presented in Fig. S14 D-F. The extracted parameters are given in Table S1.

S15 The extracted saturation current density J_s from fitting

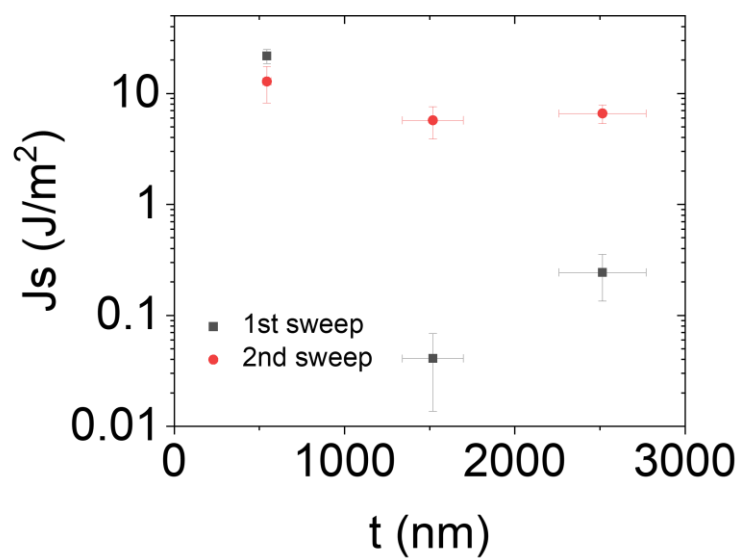


Fig. S15 The extracted saturation current density J_s against WS₂ film thickness

S16 On the hysteresis of Schottky devices

From the table S1, we can find the extracted parameters for 544 nm device show less difference between sweeps. For the rest two devices, it is found that the lower n , slightly higher ϕ_b , lower σ_{00P} from the 1st sweep compared with these from the 2nd sweep. Similar behaviors were observed in solution-processed amorphous indium gallium zinc oxide (a-IGZO) Schottky devices with a device structure of Pt/IGZO/Cu⁴. The hysteresis was ascribed to the interfacial trap states due to ionized oxygen vacancies. Although it is still unknown the origin of the surface traps in our case, the surface trap were likely gradually filled under the 1st sweep from -3 to 3 V, which causes the barrier height to be lower. For the 2nd sweep, the trap states were neutralized already, and the barrier height is close to its real value regardless of other effects. The hysteresis was also found in chemical-vapor-deposited monolayer WS₂ and it was found that charge trapping accounts for the hysteresis effect⁵. Given the complexity of solution-processed devices, there could be several factors that affect the quality of the interface. Further investigation with careful control on fabrication and testing conditions will be required.

Table S1 Extracted parameters from Schottky diodes.

Sweep	t (nm)	n	ϕ_b (eV)	σ_{OoP} (S/m)
1 st	544 ± 25	9.92 ± 0.87	0.534 ± 0.004	$6.30e-4 \pm 1.68e-4$
	1519 ± 178	1 ± 0	0.695 ± 0.021	$2.81e-5 \pm 8.87e-6$
	2515 ± 256	1.07 ± 0.14	0.648 ± 0.011	$5.98e-5 \pm 9.74e-6$
2 nd	544 ± 25	8.75 ± 0.86	0.548 ± 0.011	$6.47e-4 \pm 1.41e-4$
	1519 ± 178	7.60 ± 0.79	0.568 ± 0.009	$7.49e-4 \pm 1.85e-4$
	2515 ± 256	6.76 ± 0.19	0.564 ± 0.005	$7.31e-4 \pm 1.62e-4$

Note: t is the thickness of WS₂ film, n is the ideality factor, ϕ_b is the barrier height, σ_{OoP} is the out-of-plane conductivity.

S17 WS₂ film roughness measured by profilometry

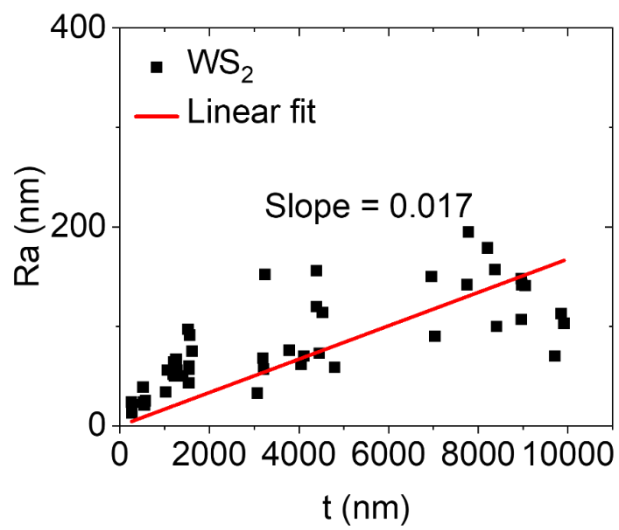


Fig. S16 WS₂ film roughness Ra as a function of its thickness t .

S18 Transition film thickness from electrode-limited to bulk-limited behaviors.

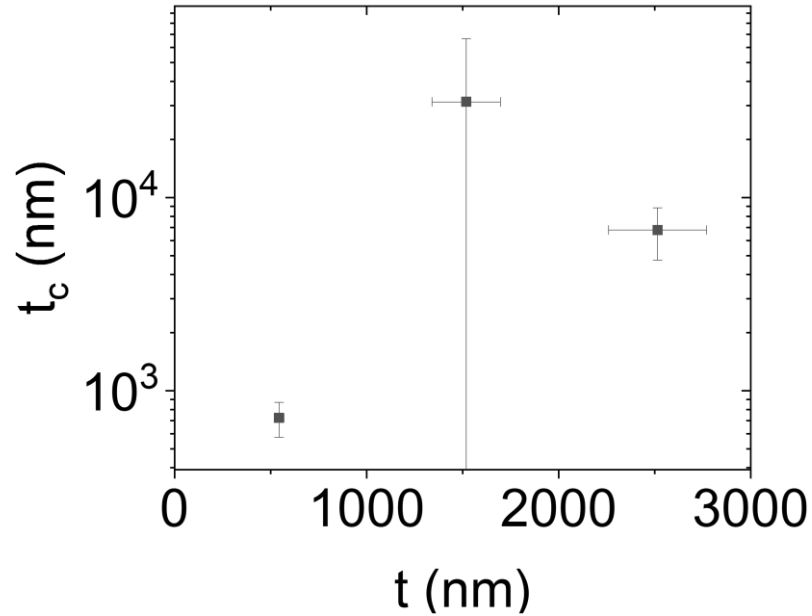


Fig. S17 Transition film thickness versus WS₂ film thickness for the data from the first sweep.

The transition film thickness t_c is determined as described in the main text. t_c from the first sweep varies from less than 1 μm to above 10 μm . This is likely due to the hysteresis effect coming from the trap states at the WS₂/S-SWNTs interfaces. In contrast, t_c obtained from the second sweep is consistent with our experimental observation as the interfacial traps are already neutralized.

Reference

1. C. Backes, B. M. Szydłowska, A. Harvey, S. Yuan, V. Vega-Mayoral, B. R. Davies, P. L. Zhao, D. Hanlon, E. J. Santos, M. I. Katsnelson, W. J. Blau, C. Gadermaier and J. N. Coleman, *ACS Nano*, 2016, **10**, 1589-1601.
2. A. G. Kelly, T. Hallam, C. Backes, A. Harvey, A. S. Esmaily, I. Godwin, J. Coelho, V. Nicolosi, J. Lauth, A. Kulkarni, S. Kinge, L. D. Siebbeles, G. S. Duesberg and J. N. Coleman, *Science*, 2017, **356**, 69-73.
3. J. C. Tinoco, M. Estrada, B. Iñiguez and A. Cerdeira, *Microelectron. Reliab.*, 2008, **48**, 370-381.
4. V. Ulianova, Y. Didenko, S. Bolat, G. T. Sevilla, D. Tatarchuk, I. Shorubalko, E. Gilshtein and Y. E. Romanyuk, *AIP Adv.*, 2020, **10**, 075104.
5. C. Lan, X. Kang, Y. Meng, R. Wei, X. Bu, S. Yip and J. C. Ho, *Nano Res.*, 2020, **13**, 3278-3285.